A THEORETICAL STUDY OF SPIN-DEPENDENT TRANSPORT IN HYBRID STRUCTURE CONSIST OF SILICON CARBIDE AND ARMCHAIR GRAPHENE NANORIBBONS

Zihab Sohbatzadeh, M.R. Roknabadi*, Nasser Shahtahmasebi, Mohammad Behdani
Department of Physics, Ferdowsi University of Mashhad, Iran
Contact address: *roknabad@um.ac.ir*

ABSTRACT: *Based on nonequilibrium Green's functions in combination with the density functional theory, a theoretical study on electronic structures and elastic spin-transport properties of a magnetic tunnel junction is presented which consists of a single iron atom adsorbed on hexagonal armchair silicon carbide nanoribbon (Fe@ASiCNR) contacted with two semi-infinite leads composed of nitrogen-doped armchair graphene nanoribbon (N-AGNR). Three different configurations are considered. The narrow Fe@ASiCNR is inserted between two AGNR electrodes doped with nitrogen at a concentration of one, two and three nitrogen impurity. The I-V characteristics of various junctions are examined, with the results exhibiting significant negative differential resistance (NDR) and spin-filter efficiency (SFE) phenomena. It is observed that such NDR effects arise from the interaction between the narrow density of states of the nitrogen-doped electrodes and discrete states in the scattering region.*

Keywords: Negative differential resistance, Spin-filter efficiency, Graphene nanoribbons, Silicon carbide nanoribbon

1. INTRODUCTION

Spintronics exploits the spin degree of freedom of electron for logic operations and information storage, which can increase data processing speed, decrease the power usage, and increase integration densities [1–3]. Graphene has attracted a lot of attention in the field of spintronics due to its unique properties such as high electronic mobility, gate tunability, and the potential for long spin lifetimes. Graphene shows long spin-scattering times, which is due to the long electronic mean-free paths, small intrinsic spin–orbit coupling and low hyperfine interaction of the electron spins with the carbon nuclei [4–6]. Graphene can also be a suitable material for spintronics and related applications which consist of spin-filter device, spin qubits, and spin-dependent field-effect transistors [7–11]. Further, Graphene derivatives are being studied in almost all fields of science and engineering. Studies show that the low-dimensional graphene nanoribbon (GNR) devices can be an excellent candidate for the future nanoelectronic devices [12–16]. There are two types of GNRs: zigzag edge nanoribbons (ZGNRs), which are cut along the zigzag dimer chain, and armchair edge nanoribbons (AGNRs), which are cut along the direction perpendicular to the zigzag dimer chain. The AGNRs are semiconductors with different band gaps depending on the width of the nanoribbons, while ZGNRs show metallic properties for all widths [17,18]. Some important AGNR-based devices such as spin filtering [19,20], negative differential resistance (NDR) [21-25], single electron characteristics, gas sensors [26], rectifying behaviors [27-30], large values of magneto resistance [31], and field-effect transistors (FET) [32] have been studied. Through various functions, NDR effect is described as the the negative slope of current-voltage curve. It is recognized that NDR holds great promising due to its possible utilization in multi-valued memory circuits and high-speed devices [33].

Chemical functionalization [34], adsorption [35], impurity doping [36], and defects [37] have been revealed to be the leading elements that determine the electronic transport properties of GNRs at nanodevices. Zhou et al. [38] examined the NDR phenomena by investigating the electronic transport properties of P-doped AGNRS lead. Huang et al. [39] explored the transport properties through FeN4, alkane (C5), and benzene molecules sandwiched between two N-doped zigzag and armchair GNRs, finding that robust NDR effect appeared in all examined molecular junctions. They reported that the narrow density of states of N-doped GNRs and the bias-dependent effective coupling between the discrete frontier molecular orbitals and the subbands of electrodes were responsible for the observed NDR behavior. Padilha and colleagues [40] showed that the system composed of a zig-zag hexagonal boron nitride nanoribbon contacted by two zig-zag graphene nanoribbons could act as spin-filter (the efficiency reaches 50%), depending on the length of the boron nitride region.

To our knowledge, there is a paucity of theoretical reports on iron odsorbed into hybrid structures in the literatures. In the present work, a magnetic tunnel junction consisting of a single iron atom adsorbed on hexagonal armchair silicon carbide nanoribbon (Fe@ASiCNR) contacted with two semi-infinite leads composed of nitrogen-doped AGNR (N-AGNR) is investigated. Based on ab initio transport calculations, it is predicted that such a system can be used to build NDR devices, acting as a spin-filter.

2. COMPUTATIONAL METHODS

The structural relaxations and electronic properties are calculated using the spin-polarized DFT implemented in the SIESTA code [41]. In our simulations, the generalized gradient approximation (GGA) is used to describe the exchange and correlation energy. The structural relaxations of each two-probe system have a force tolerance of 0.05 eV/Å. The wave functions of the valence electrons are expanded by a linear combination of atomic orbitals (LCAO). To describe the interactions of the ionic cores and valence electrons, norm conserved pseudopotentials proposed by Troullier–Martins [42] was used. A double-zeta polarized basis set (DZP) was adoped for all atoms including C, N, Si, and Fe atoms. An energy cutoff of 300 Ry for the grid integration was used in

the real space. A sample of 1 × 1 × 9 k-points chosen based on the Monkhorst-Pack method was used to describe the Brillouin zone [43]. A vacuum layer larger than 15 Å was used to prevent the interaction of adjacent ribbons.

The transport properties through the Fe adsorbed ASiCNRs sandwiched between two N-doped AGNR electrodes were investigated using standard DFT calculations combined with non-equilibrium Green's functional technique, which were performed in TRANSIESTA code [44]. In these calculations, the total transmission coefficients were given by

$$T^{\sigma}(E,V) = Tr[\Gamma_L G_{\sigma} \Gamma_R G_{\sigma}^{+}]$$

where, σ stands for the spin-up and spin-down channels, $\Gamma_{L/R}$ is the coupling matrix between the scattering region and left/right electrode and G_{σ} is the retarded Green's function of the scattering region. Landauer-Buttiker formula is used to calculate the spin-polarized current through the system [45],

$$I^{\sigma}(V) = \frac{2e}{h} \int_{U_L(V)}^{U_R(V)} f[E - U_L(V)]\, f[E - U_R(V)] T^{\sigma}(E,V) dE$$

Here, e is the electron charge, h is Planck's constant, *f* is the Fermi–Dirac function, and $U_L(V)$ and $U_R(V)$ are the chemical potential of the left and right leads respectively. Under the external bias voltage V, $U_{L/R}(V)$ shifts rigidly downward (or upward) by V/2 relative to each other, namely $U_{L/R}(V) = E_F \pm eV/2$, where E_F stands for the chemical potential of left/right electrode, which is set to zero in all the calculations.

In Fig. 1(a), a schematic view of the system before relaxation has been shown. The device is divided into three parts including the left lead, scattering region, and the right lead. Two semi-infinite nitrogen-doped AGNRs (N-AGNRs) are used to model the left and right electrodes. Figs. 1(b), (c) and (d) illustrate the N-AGNR electrode with a width of (w = 6) labeled as 6-AGNR. Each lead is described by a super cell along the transport direction. The iron-adsorbed is located near the edge region of ASiCNR (Fe@ASiCNR) to produce the adsorbed states close to the Fermi level. The scattering region consists of the Fe@ASiCNR and the surface layers of the left and right electrodes, where all screening effects are included in the contact regions. The length of the SiCNR is about 3.61Å. Here, it is assumed that the electrodes only couple with the central scattering region, not with each other.

After the relaxation of each structure, a view of the systems under study is shown in Fig. 2. As can be seen, the structural symmetry is broken when a narrow Fe@ASiCNR is inserted between two N-AGNRs. (a), (b) and (c) represent iron adsorbed hybrid AGNR-SiC-GNR nanoribbon doped with nitrogen at a concentration of one, two and three nitrogen impurity, i.e. A, B and C structures, respectively (Figs. 2(a), 2(b), and 2(c)).

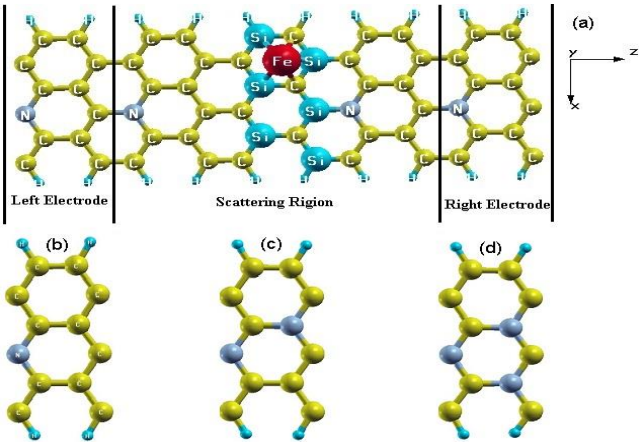

Fig. 1. (a) Schematic view of the system before relaxation. This system is flat in the z-x plane, with 6-armchair chains along the z-direction. Iron adsorbed armchair hexagonal silicon carbide nanoribbon contacted with two semi-infinite nitrogen-doped armchair graphene nanoribbon electrodes. The device was divided in three parts: a left-hand and a right-hand side electrode, a central scattering region composed of a few unit cells of the electrodes and a unit cell of an armchair hexagonal silicon carbide nanoribbon. (b), (c) and (d) the unit cells of nitrogen doped 6AGNR with three doping cases, respectively. One to three carbon atoms in a six-number ring are subsitutionally doped as an alternate in each supercell by nitrogen atoms

3. RESULTS AND DISCUSSION

Before investigating the transport properties of considered configurations, we first calculate the band structures and density of states (DOS) of N-doped and undoped GNRs for the 6N-AGNR electrode. The effects of doping on the electronic and magnetic structures and the properties of AGNR doped by nitrogen atoms are the result of interactions between the doping atoms and their neighbors. We start with three nitrogen doping configurations, where each case has a different supercell size, and one to three carbon atoms in a six-number ring are substitutionally doped in each supercell, by alternate nitrogen atoms. (Figs. 1(b), (c) and (d)). Although nitrogen impurities in π-conjugated systems can affect the magnetic properties of the material [46], but in our calculations, the spin polarization in these electrode configurations is negligible.

The bandgaps of hydrogen-passivated N_a-AGNRs are divided into three different groups based on the value of N_a [47]. For a given integer m, the group is $N_a = 3m + 2$, and other groups are $N_a = 3m + 1$ and $N_a = 3m$. Therefore, 6-AGNR is selected as the model system to investigate the consequence of an isolated subsitutionally doped nitrogen atom on AGNRs.

The electronic band structures of three selected N-AGNR structures are shown in Figs. 3(b), (c) and (d), which correspond to Figs 1(b), (c) and (d) respectively. The pristine band structure [Fig. 3(a)] is also shown for the purpose of comparison. An analysis of electronic band structures depicts that the existence of nitrogen impurity eliminates the intrinsic semiconductivity of pristine AGNR. Nitrogen adatom can lead to the distortion of the AGNR upon adsorption, which possibly brings about a change from an AGNR sp^2 –like orbital character to a more covalently sp^3 -like one. Nitrogen

doping produces a positive shifting of Fermi energy due to the extra π electrons from the nitrogen atom.

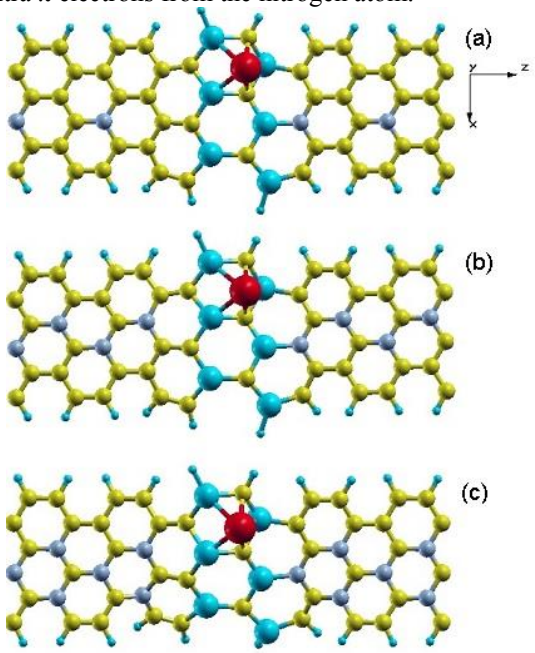

Fig.2. Schematic representation of the various configurations used in calculations after the relaxation of each structure. The structural symmetry is broken when a narrow Fe adsorbed armchair SiC nanoribbon is inserted between the two N-doped armchair graphene nanoribbons. (a), (b) and (c) represent one, two and three nitrogen doping on iron adsorbed hybrid AGNR-SiC-GNR nanoribbon, i.e. A, B and C structures respectively.

The conduction-band structure is perturbed by the impurity nitrogen atom while valence-band structure generally remains unperturbed compared to pristine AGNR. In addition, for nitrogen-doped 6-AGNR, it is found that the energy bands are degenerated at the zone boundary.

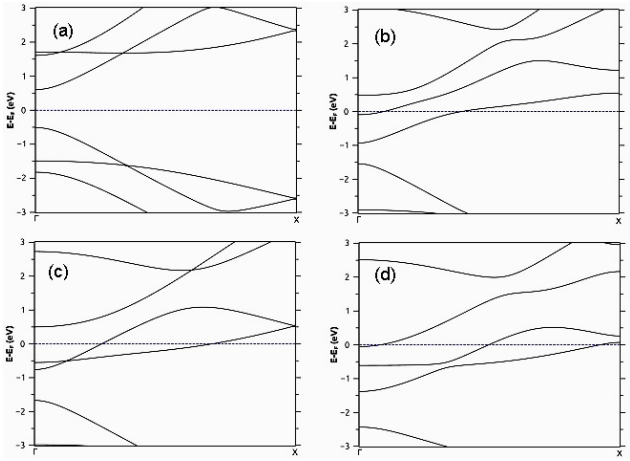

Fig. 3. Calculated band structures of 6AGNR in (a) pristine, (b), (c) and (d) one, two and three nitrogen-doped respectively. The Fermi energy is set at 0 eV.

In order to better understanding of electronic properties, the density of states (DOS) have been plotted in Fig. 4. The semiconducting nature of pristine AGNR is well defended by the electron density gap at Fermi energy in the DOS [Fig. 4(a)]. Nitrogen- doped AGNRs [see Figs. 1(b), (c) and (d)] are metallic because there are narrow DOS that cross the Fermi level due to the presence of the substituted nitrogen dopant. That is, semiconducting undoped AGNRs can be converted into metal by the doped nitrogen atom. These investigations show that nitrogen-doped GNRs with armchair edges are excellent conducting electrodes [48].

Now, we turn to examine the transport properties of three considered systems with nitrogen-doped 6-AGNRs electrodes. Figs. 5 (a), (b) and (c) show spin-resolved I-V curves of all configurations in the bias voltage (V_{bias}) in a range of 0.0 to 1.2 V in a step of 0.1 V. Here, the currents of spin-up and spin-down electrons are plotted with black and red lines, respectively. At each bias voltage, the current is determined self-consistently under the non-equilibrium condition. As can be seen, these systems display obvious spin-filtering behavior. Within V_{bias} range of 0.0 to 1.2 V, the current of the spin-down electrons (I↓) is considerably larger than that of spin-up electrons (I↑).

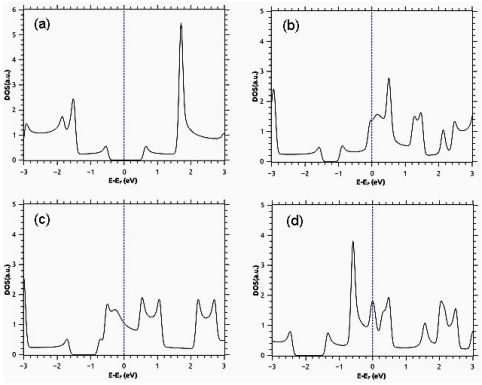

Fig. 4. The calculated DOS of 6AGNR in (a) pristine, (b), (c) and (d) one, two and three nitrogen-doped respectively. The Fermi energy is set at 0 eV.

The negative differential resistance (NDR) behaviors is evident in all cases.

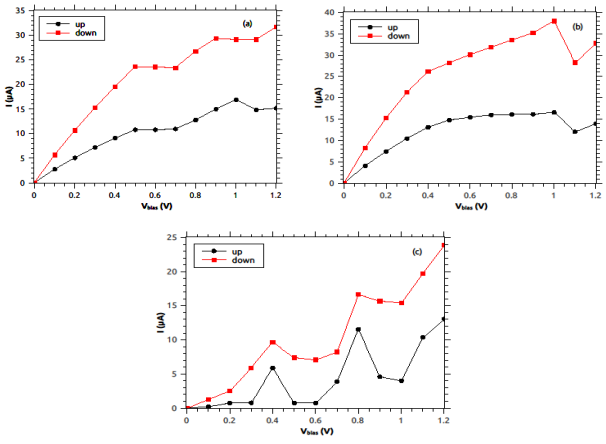

Fig. 5. Comparing the characteristics of the spin-dependent current–voltage (*I–V*) of the (a), (b) and (c) one, two and three nitrogen doping on iron adsorbed hybrid AGNR-SiC-GNR nanoribbon, respectively (A, B and C structures)

The *I-V* curve of A system, as shown in Fig. 5(a), indicates that I↑ initially increases by applying V_{bias}. Then, a regime with NDR phenomena appears in a voltage range of 1.0 to 1.2 V. The maximum current of the spin-up electrons is up to about 16.86 μA at the peak position (V_{bias} = 1.0 V), while it reaches its minimum value (14.84 μA) at the valley site (V_{bias} = 1.2 V). For the spin-down electrons, it is observed that NDR character is negligible and the current increases by applying V_{bias}. The current peak-to-valley ratio (PVR), which is defined as PVR = I_{peak}/I_{valley}, is often used to describe NDR effect, with PVR being predicted to be 1.13 for the spin-up electrons. As indicated in Fig 5(b), the corresponding NDR behavior is also observed in B system at the same voltage range (1.0 to 1.2 V). The spin-up (down) current of this system increases when the value of the applied bias is between V_{bias} = 0 V and V_{bias} = 1.0 V. If the applied voltage is beyond 1.0 V, the current decreases and NDR phenomena appears in a voltage range of 1.0 to 1.2 V. Moreover, it is observed that PVR reaches 1.37 and 1.34 for spin-up and spin-down channels, respectively. In the case of C system, two significant NDR behaviors are indicated in two bias voltage ranges: 0.4 to 0.6 V and 0.8 to 1.0 V. In the first bias voltage, PVR reaches the maximum value of 8 for spin-up and 1.36 for spin-down channels, whereas in the second range, the value of the PVR is estimated between 2.88 and 1.07 for the spin-up and spin down channels respectively.

To illustrate the mechanism of NDR phenomena, for example, we take the C configuration. We studied the electronic structures of periodic electrodes and the isolated scattering region. The calculated density of states (DOS) of nitrogen-doped AGNRs electrodes, and the DOS of the isolated regions are shown in Fig. 6. As can be seen, there are two obvious narrow DOS peaks (labeled with A and B) of nitrogen-doped electrode. These two narrow peaks apparently arise from nitrogen doping, in which one more electron is introduced into the system per unit cell. The isolated scattering region with all dangling bonds saturated by hydrogen atoms possesses two states near the Fermi level (labeled with C and D) which can act as two tunneling channels. When a bias voltage is applied, the relative position of narrow peaks in DOS of electrodes is shifted. In the resonant tunneling process, the junction becomes conductive when the energy position of channel state(s) in the electrodes matches that of the channel(s) in the scattering region. However, when the bias voltage increases continuously, those well-matched states can become mismatched. Therefore, the current first increases through the scattering region and then decreases, leading to an NDR peak.

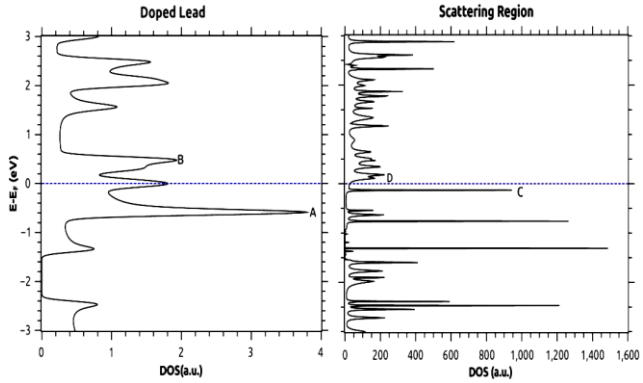

Fig. 6. The calculated DOS of N-doped ANGRs, and the energy levels of the isolated scattering region saturated by hydrogen atoms. When a bias voltage is applied, the relative position of narrow peaks in DOS of leads (A and B) is shifted. In the resonant tunneling regime, the junction becomes conductive when the energy position of channel state(s) in the scattering region (C and D) matches that of channel(s) in the electrodes.

To shed further light on the NDR mechanism, it should be noted that NDR effect can be associated with changes of coupling between the scattering region orbitals and incident states in the electrodes under various biases. As noted in the Landauer-Buttiker formula, in the computational method section, the current flowing through a device can be determined by integrating the transmission function *T(E)* in the integral window (bias window). For example, to explain the NDR effect observed at the spin-up *I–V* curve of C system (Fig. 5(c)), we calculate the *T(E)* at bias voltages of 0.0, 0.4, 0.6 and 0.7 V. The energy range associated with the voltage applied between the two electrodes is specified by dashed lines, as indicated in Fig. 7. As can be seen, by increasing the bias voltage from 0.0 to 0.4 V, the transmission region becomes wider (Figs. 7(a) and (b)). This is due to the fact that the electrons can be transmitted from the higher energy regions of the left electrode through the device to the lower energy regions of the right electrode in an increasingly wider energy region. Therefore, the current through junction increases in this bias voltage, as indicated in Fig. 5(c). The behavior of transmission function varies significantly when the bias voltage increases continuously to 0.6 V. As shown in Fig. 7(c), in a range of energy from -0.3 to 0.3 eV, the transmission coefficients are negligible. Again, when the bias voltage increases to 0.7 V, the transmission coefficients will be considerable (Fig 7(d)). As a result, the current in the voltage range of 0.4–0.6 V decreases dramatically, indicating NDR effect in this voltage range.

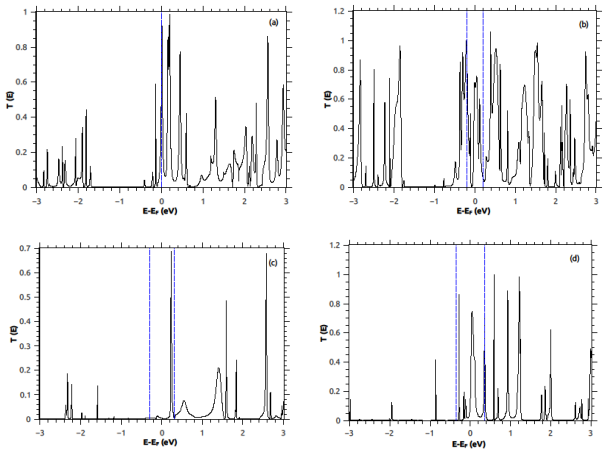

Fig. 7. The changes of the transmission function under various biases of C system for the bias voltage of (a) 0.0 V, (b) 0.4 V, (c) 0.6 and (d) 0.8 V. The dashed line shows the bias window.

The transport currents of all configurations are spin-polarized, as displayed in Figs. 5(a), (b) and (c). In the following, spin-filter effects are further studied in a bias range from 0.1 to 1.2 V. The spin-filter efficiency (SFE) η defined at finite bias as follows:

$$\eta = \left| \frac{I_{up} - I_{down}}{I_{up} + I_{down}} \right| \times 100$$

Where $I_{up(down)}$ indicates the spin-up (spin-down) current at the finite bias, respectively.

As shown in Fig. 5, for all configurations, the current of spin-down (I_{down}) is larger than that of spin-up (I_{up}), because the value of T_{down} is greater than that of T_{up}. Thus, given that the value of SFE is negative in all systems, we have used its absolute value in our discussions.

To understand the origin of negative SFE, it is necessary to study the transmission spectrum at some bias voltages. We take the C structure as an example. Figs. 8(a) and (b) show the spin-resolved transmission spectra of considered system at V_{bias} = 0.5 and 0.9 V respectively. The transmission coefficients of the spin-down electrons are often higher than those of spin-up electrons in the bias window at selected bias voltages. this is consistent with negative SFEs (-54.73 and -81.12 %, respectively) under these biases.

The large magnitude of spin-filter efficiency in the C structure (81.58%) suggests possible applications such as spin filter devices. This behavior would be suitable for a spin current switch. As shown in Fig. 9(a), it should be noted that there is a significant SFE in the A structure. The values of SFE at V_{bias} = 0.4 and 0.5 V are 36.64 and 37.28% respectively. As such, although spin-filter efficiency in the B structure is insignificant at above-mentioned biases, at other biases, V_{bias} = 1.1 and 1.2 V shows a considerable magnitude of 40.28 and 40.27%, respectively.

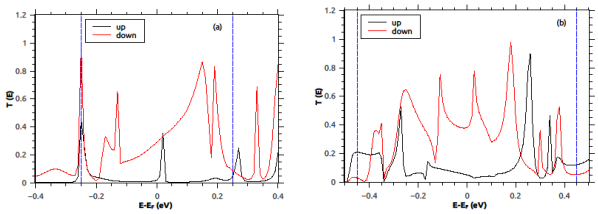

Fig. 8. Spin-polarized transmission spectra at (a) V_{bias} = 0.5 V and (b) V_{bias} = 0.9 V. The dashed blue lines denote the bias window.

The calculated spin-filter efficiency (SFE) η of considered devices are plotted in Figs. 9(a), (b) and (c). As can be seen, SFEs are all highly sensitive to the bias voltage. In all studied systems, the maximum values of SFE oscillated around 36-81%.

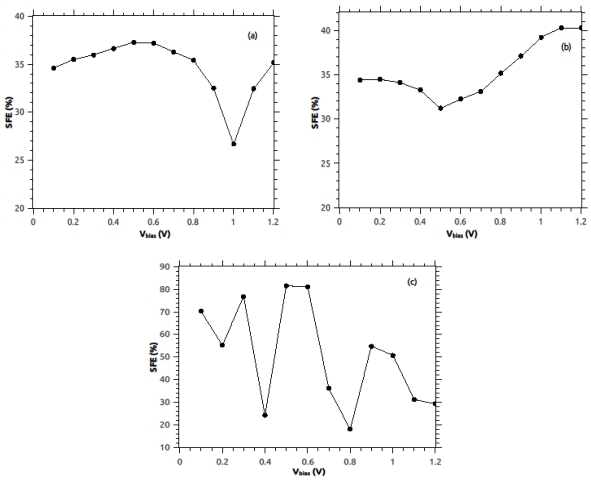

Fig. 9. Bias-dependent spin filter efficiency (SFE) of (a), (b) and (c) one, two and three nitrogen doping on iron adsorbed hybrid AGNR-SiC-GNR nanoribbon respectively (A, B and C structures).

As pointed out earlier, it is worth mentioning that C configuration, compared to other structures, is capable of producing a significant spin-polarized transport. As a result, the highest SFE is observed in this configuration.

The spin-resolved current indicates that the analyzed structures are suitable either for spin-filter applications or for spin-current switching devices.

4. . CONCLUSION

In this study, we have explored electronic structures and spin-transport properties of hybrid nanoribbons by examining three different configurations. The narrow Fe@ASiCNR is inserted between two AGNR electrodes doped with nitrogen at a concentration of one, two and three nitrogen impurity. The results show that the significant NDR effect is arised from the narrow DOS peaks of the N-doped electrodes and discrete states of the scattering region. The maximum peak-to-valley ratio is about 8, which is obtained in the case of electrode doped with three nitrogen impurity (C configuration). Also, it should be pointed out that in addition

to NDR, spin-filtering effect appears in all examined configurations and the predicted spin-filter efficiency is up to 80% in the C configuration. The results show that the doping concentrations play an important role in the NDR and SFE effect of the studied devices. These findings suggest that iron adsorbed hybrid AGNR-SiC-GNR nanoribbon doped with nitrogen can be a suitable candidate for future applications in electronic circuits, molecular spintronics devices such as spin-filter, molecular switches, and molecular memories.

REFERENCES

[1] Wolf SA, Awschalom DD, Buhrman RA, Daughton JM, Molnar SV, Roukes ML, et al. Science 294 (2001) 1488.

[2] Zutic I, Fabian J, Sarma SD, Rev. Mod. Phys. 76 (2004) 323.

[3] Chappert C, Fert A, Dau FNV. The emergence of spin electronics in data storage. Nat Mater. (2007) 813.

[4] Tombros N, Jozsa C, Popinciuc M, Jonkman HT, Wees BJW, Nature 448 (2007) 571.

[5] Han W, Kawakami RK, Phys. Rev. Lett. 107 (2011) 047207.

[6] Ma DW, Li ZY, Yang ZQ. Strong , Carbon 50 (2012) 297.

[7] Trauzettel B, Bulaev DV, Loss D, Burkard G. Nat Phys. 3 (2007) 192.

[8] Avsar A, Yang TY, Bae S, Balakrishnan J, Volmer F, Jaiswal M, et al. Nano Lett. 11 (2011) 2363.

[9] Gunlycke D, White CT. Phys. Rev. Lett. 106 (2011) 136806.

[10] Zeng MG, Shen L, Zhou M, Zhang C, Feng YP. Phys. Rev. B 83 (2011) 115427.

[11] Yazyev OV. Phys. Rev. Lett. 100 (2008) 047209.

[12] Y. Son, M. L. Cohen, and S. G. Louie, Nature 444 (2006) 347.

[13] Y. Son, M. L. Cohen, and S. G. Louie, Phys. Rev. Lett. 97 (2006) 216803.

[14] R. Goeckeritz, J. Pezoldt, and F. Schwierz, Appl. Phys. Lett. 99 (2011) 173111.

[15] Modarresi M, Roknabadi MR, Shahtahmassebi N, Physica E 44 (2012) 1214.

[16] Modarresi M, Roknabadi MR, Shahtahmassebi N, Physica B 415 (2013) 62.

[17] Y. P. An, W. Ji, and Z. Q. Yang, J. Phys. Chem. C 116 (2012) 5915.

[18] V. Nam Do and P. Dollfus, J. Appl. Phys. 107 (2010) 063705.

[19] J. Kang, F. Wu, and J. Li, Appl. Phys. Lett. 98 (2011) 083109.

[20] Zihab Sohbatzadeh, M.R. Roknabadi, Nasser Shahtahmasebi, Mohammad Behdani, Physica E 65 (2015) 61.

[21] J. Chen, M. A. Reed, A. M. Rawlett, and J. M. Tour, Science 286 (1999) 1550.

[22] H. Ren, Q. X. Li, Y. Luo, and J. L. Yang, Appl. Phys. Lett. 94 (2009) 173110.

[23] Modarresi M, Roknabadi MR, Shahtahmasbi N, Vahedi D, Arabshahi H, Physica E 43 (2010) 402.

[24] M. Modarresi, M.R. Roknabadi, N. Shahtahmassebi, Physica B 415 (2013) 62.

[25] Masoud Darvish Ganji, Zihab Sohbatzadeh and Azadeh Khosravi, Struct.Chem. 25 (2014) 551.

[26] Y. H. Zhang, Y. B. Chen, K. G. Zhou, C. H. Liu, J. Zeng, H. L. Zhang, and Y. Peng, Nanotechnology 20 (2009) 185504.

[27] C. Cao, L. N. Chen, M. Q. Long, and H. Xu, Phys. Lett. A 377 (2013) 1905.

[28] J. G€uttinger, F. Molitor, C. Stampfer, S. Schnez, A. Jacobsen, S. Dr€oscher, T. Ihn, and K. Ensslin, Rep. Prog. Phys. 75 (2012) 126502.

[29] X. Q. Deng, Z. H. Zhang, G. P. Tang, Z. Q. Fan, M. Qiu, and C. Guo, Appl. Phys. Lett. 100 (2012) 063107.

[30] J. Zeng, K. Q. Chen, J. He, Z. Q. Fan, and X. J. Zhang, J. Appl. Phys. 109 (2011) 124502.

[31] F. Munoz-Rojas, J. Fernandez-Rossier, and J. J. Palacios, Phys. Rev. Lett. 102 (2009) 136810.

[32] W. Y. Kim and K. S. Kim, Nat. Nanotechnol. 3 (2008) 408.

[33] J. Chen, M. A. Reed, A. M. Rawlett, and J. M. Tour, Science 286 (1999) 1550.

[34] V. A. Rigo, T. B. Martins, A. J. R. da Silva, A. Fazzio, and R. H. Miwa, Phys. Rev. B 79 (2009) 075435.

[35] S. Dutta and S. K. Pati, J. Phys. Chem. B 112 (2008) 1333.

[36] J. Berashevich and T. Chakraborty, Phys. Rev. B 80 (2009) 033404.

[37] D. W. Boukhvalov and M. I. Katsnelson, Nano. Lett. 8 (2008) 4373.

[38] Yuhong Zhou, Jianbing Zhang, Daoli Zhang, Cong Ye, and Xiangshui Miao, J. Appl. Phys. 115 (2014) 013705.

[39] Jing Huang, Weiyi Wang, Qunxiang Li, and Jinlong Yang, J. Chem. Phys 140 (2014) 164703.

[40] José Eduardo Padilha, Renato Borges Pontes, Antônio José Roque da Silva, Adalberto Fazzio, Solid. State Commun. 173 (2013) 24.

[41] J. M. Soler, E. Artacho, J. D. Gale, A. Garcia, J. Junquera, P. Ordejon, and D. S. Portal, J. Phys.: Condens. Matter 14 (2002) 2745.

[42] N. Troullier, J.L. Martins, Physical Review B 43 (1991) 1993.

[43] Monkhorst, H. J.; Pack, J. D. Phys Rev B 13 (1976) 5188.

[44] J. M. Soler, E. Artacho, J. D Gale, A. Garcia, J. Junquera, Pablo Ordejon and D. Sanchez-Portal, J. Phys.: Condens. Matter 14 (2002) 2745.

[45] M. B€uttiker, Y. Imry, R. Landauer, and S. Pinhas, Phys. Rev. B 31 (1985) 6207.

[46] I. Hagiri, N. Takahashi, K. Takeda, J. Phys. Chem. A 108 (2004) 2290.

[47] Y.-W. Son, M. L. Cohen, and S. G. Louie, Phys. Rev. Lett. 97 (2006) 216803.

[48] H. Ren, Q. X. Li, Y. Luo, and J. L. Yang, Appl. Phys. Lett. 94 (2009) 173110.